The "Porcupine": A Novel High-Flux Absorber For Volumetric Solar Receivers

J. Karni, A. Kribus,
R. Rubin, P. Doron
Department of Environmental Sciences
and Energy Research
The Weizmann Institute of Science
Rehovot 76100, ISRAEL

A new Volumetric (Directly-Irradiated) solar absorber, nicknamed Porcupine, is presented. It was tested over several hundreds of hours at the Weizmann Institute's Solar Furnace, using several flow and geometric configurations, at various irradiation conditions. The experiments, which were conducted at a power level of about 10 kW, showed that the new absorber can accommodate different working conditions and provide a convective cooling pattern to match various irradiation flux distributions. The capability of the Porcupine to endure a concentrated solar flux of up to about 4 MW/m^2, while producing working gas exit temperatures of up to 940°C, was demonstrated. In comparative tests, the Porcupine sustained an irradiation solar flux level about 4 times higher than that sustained by other Volumetric absorbers (foam and honeycomb matrices). Due to its ability to sustain and transport a much higher energy fluxes, the Porcupine yielded twice the power output of the other absorbers while its exit gas temperature was 300–350°C higher. The Porcupine design is highly resistant to thermal stresses development; none of the Porcupine absorbers tested showed any sign of deterioration after hundreds of operating hours, although temperature gradients of several hundreds °C/cm developed in some experiments. The basic Porcupine structure provides convective and radiative energy transport between the matrix elements, therefore alleviating the development of flow instabilities; this phenomenon causes local overheating and restricts the operation of other Volumetric matrices. A Porcupine absorber was subsequently incorporated into the Directly Irradiated Annular Pressurized Receiver (DIAPR), where it has been operating flawlessly at an incident flux of several MW/m^2 and temperatures of up to 1,700°C.

Introduction

A Solar Receiver is the component of a solar-thermal system where concentrated sunlight, provided via an optical concentrator, is absorbed and converted to thermal energy or chemical potential. The receiver design depends on the type of concentrator (e.g., trough, parabolic dish, heliostat field), the working fluid, and the operating ranges of temperature, pressure and radiation flux. In systems such as a parabolic dish or a central receiver the concentration ratio is typically high, over 100 times of the normal sunlight reaching the earth. The temperatures are also quite high: ranging from 500 to 1,300°C for various applications. As the temperature, pressure and solar flux increase, it becomes more difficult to effectively handle the concentrated solar energy provided by the optical system, and the receiver design poses a greater challenge. Material properties, for example, determine the maximum receiver temperature, and may also force the designer to lower the working pressure, as the receiver temperature increases.

Most of the solar receivers can be classified as either *Indirectly-Irradiated* or *Directly-Irradiated (Volumetric)*. The common characteristic of the *Indirectly Irradiated* receivers is that the heat transfer to the working fluid does not take place upon the surface which is exposed to incoming solar radiation. Instead, there is an intermediate wall, which is heated by the irradiated sunlight on one side and transfers the heat to a working fluid on the other side. The two main groups of Indirectly-Irradiated receivers are *Tubular Receivers* (Smith and Allman, 1990; Epstein, 1990; Litwin and Rogers, 1996) and *Heat Pipe Receivers* (Doerte and Goebel, 1992; Diver et al., 1992; Klimas et al., 1992; León et al., 1994; Andraka et al., 1995; Noble et al., 1995). All these receivers are limited to a working fluid temperature below 1,000°C and a solar flux of less than 1,000 kW/m^2. Due to material and design limitations, an increase in the operating temperature poses more severe restrictions on the pressure and the solar flux. For example, at the upper temperature range of Indirectly-Irradiated receivers (T>800°C) the flux and pressure cannot exceed 600 kW/m^2 and 10 bar, respectively.

In Volumetric, or *Directly-Irradiated*, receivers the heat transfer to the working fluid takes place upon the surface which is heated directly by incoming radiation. Receivers of this diverse group have been developed for both parabolic dish and central receiver systems (Flamant and Olalde, 1983; Hunt and Brown, 1984; Fricker et al., 1990; Chavez et al., 1990; Pitz-Paal et al.,

Nomenclature

C	Cumulative flux concentration ratio: power incident on a circle of radius r, divided by the circle's area and by the normal insolation I_n	$\dot{m}$	Mass flow rate (kg/s)
D	Correction factor for Furnace door opening	O	Furnace door opening (m)
I_n	Direct normal insolation (W/m^2)	Q	Power (W)
$I_{abs}(r)$	Averaged flux absorbed and transferred to the gas within a circle with radius r (W/m^2)	r	Radius (mm)
L	Distance behind focal point (mm)	R	Overall absorber radius (mm)
		T	Temperature (°C)
		η	Efficiency
		τ	Transmissivity of the bell-jar

1991; Buck, 1990; Pritzkow, 1991; Anikeev et al., 1992; Posnansky and Pylkkänen, 1992; Chavez et al., 1994; Abele et al., 1996; Buck et al., 1996). In general, the flux, working pressure and temperature achieved by these receivers have not exceeded those of tubular receivers. The only receiver so far to demonstrate a significant advance in operating conditions is the *Directly Irradiated Annular Pressurized Receiver* (DIAPR), tested successfully under incident flux of over 5,000 kW/m^2, while delivering air at a temperature and pressure of 1,200°C and 20 bar, respectively (Karni et al., 1996; Karni et al., 1997). Such temperature and pressure allow utilization of solar energy to drive modern turbomachinery and various high-temperature thermochemical processes. As the operating temperature increases, the incident solar flux must also increase to reduce reradiation losses (Fletcher and Moen, 1977).

A key element of all Directly-Irradiated receivers is the absorber: the component which absorbs concentrated sunlight and transports its energy to a working fluid flowing within and over it. In different designs, the absorber is either located adjacent to the receiver aperture, or deeper in the receiver cavity. It is either a stationary matrix (grid, wire-mesh, foam, honeycomb, etc.), or moving (usually solid) particles. Directly-Irradiated receivers with stationary absorbers are relatively simple and the most common of the Volumetric receiver family. Here, the absorbing matrix must be able to absorb highly concentrated radiation, while providing sufficient heat convection to the working gas flow. It is also required to sustain thermal stresses created by large temperature gradients as well as thermal shock caused by rapid heating-cooling cycles.

Often the operating conditions demand that the absorber be physically separated from the ambient; e.g., when the flow is pressurized, or the working fluid is not air. In these cases the receiver must be equipped with a transparent window, which allows concentrated light to enter the receiver, while separating the working gas and the ambient air (Pritzkow, 1991; Buck et al., 1996; and Karni et al., 1997).

Both metal and ceramic absorbers have been studied. Early tests of an open-air (windowless) receiver with a metallic wire-pack absorber were conducted by Fricker et al. (1990). The main advantage of this type of a receiver is its simplicity. The absorber, which is located at or just behind the aperture is the only main component in the receiver. Ambient air is sucked in through the absorber, which is exposed to concentrated solar radiation. The main problems are the control of the insolation and air flow across the absorber to prevent local overheating, and the design of an effective, durable absorber. This receiver was later modified and scaled up to a 2.5 MW size model, which was built and tested as part of the PHOEBUS project (Heinrich et al., 1992; Haeger et al., 1994). The absorber of the latter receiver was made of a non-uniform metal grid, having narrower opening near the center, where the concentrated solar flux was relatively high. The flow distribution across the absorber was controlled by perforated plates, located behind it. The PHOEBUS absorber was designed for an average incident solar flux of 500 kW/m^2, peak flux of 800 kW/m^2 and exit air temperature of 700°C.

Chavez et al. (1994) proposed and tested a Nichrome (80% nickel, 20% chrome) wire mesh absorber capable of a somewhat better performance than that of the PHOEBUS absorber, due to the improvement in absorber material. Another metal (X5CrAl205+Ce) absorber matrix, CATREC I & II, was proposed by Pitz-Paal (1996); the latter version of this absorber was able to withstand temperatures of over 1,050°C, but the exit air temperature achieved in the tests was only 440°C. Improvements are expected with better control and matching of the air flow and the solar flux distribution on the absorber; similar methods to those used in the PHOEBUS receiver tests can be implemented. Böhmer and Chaza (1991) and Pitz-Paal et. al. (1991) proposed a ceramic (Si-SiC) foil absorber, shaped like a honeycomb. This absorber produced air temperatures of over 800°C at a mean solar flux of 250 kW/m^2. Levy et. al. (1989) used a catalytic honeycomb absorber for CO_2–CH_4 reforming. Helmuth et. al., (1994) investigated an absorber made of layers of wire mesh, with a different opening size. This design can improve the penetration of irradiation into the absorber. Olalde et. al. (1985), Menigault (1991) and Pitz-Paal et. al. (1992) attempted to improve the penetration of sunlight into the absorber using two-stage absorbers, where the front part, facing the irradiation, is made of a selectively transparent material. Buck (1990) constructed an absorber with thin SiC fibers; subsequent work from the same laboratory employed metallic screen and ceramic (SiC and Si_3N_4) foam absorbers of various configurations (Pritzkow, 1991; Buck et al., 1991; Bauer et al., 1994; Abele et al., 1996; Buck et al., 1996).

In a recent analysis, Kribus et al. (1996) found that in a stationary absorber, where the flow is nearly one-dimensional and in parallel channels (e.g., foam, honeycomb, grid), there is a potential for flow instability related to fluid property changes; this may cause local overheating and therefore restricts the concentration of the incoming solar radiation. Hoffschmidt et al. (1996) reported that similar intrinsic instabilities, which increase with irradiation flux and absorber temperature, were observed in a number of tests. Pitz-Paal et. al (1997) used different experimental and numerical results to analyze the effect of non-homogeneous irradiance distribution on the flow and temperature instabilities of the absorber. They concluded that the presence of effective lateral mixing, by flow having a significant component perpendicular to the main flow direction, and substantial lateral radiation exchange between the absorbing elements, would reduce or even eliminate this problem.

In the aforementioned volumetric absorbers radiation exchange between the elements is limited, and the flow is either strictly one-dimensional, or there is limited lateral mixing. They are therefore susceptible to this thermal instability mechanism and the formation of 'hot spots' (i.e., local temperature peaks, much higher than the average absorber temperature). Furthermore, the structure of the above absorbers is basically rigid so they can sustain only marginal stresses developed due to temperature variations. Absorber durability and longevity have therefore been a major problem, in addition to the performance limitations. The methods used to stabilize and improve absorber operations are (Haeger et. al., 1994; Abele et. al., 1996; Buck et. al., 1996; Pitz-Paal et al., 1997):

- strict, continuous control of the incoming radiation, assuring that the local flux does not exceed a prescribed concentration limit;
- varying the pore size in the absorber's porous matrix according to the designed flux distribution;
- control of the flow through the absorber by placing quadratic-resistance elements (e.g., a non-uniform perforated plate) behind the absorber.

With these modifications the maximum operating conditions achieved by volumetric absorbers were peak incident solar flux of about 1000 kW/m^2 (Buck et. al. 1996) and exit gas temperature approaching 1000°C (Pitz-Paal et. al., 1997).

Development of the *Porcupine* absorber was aimed at producing an absorber matrix capable of operating over large and variable conditions; therefore, it must have the following characteristics:

- allow penetration of incident radiation into it and provide good radiative exchange between the absorbing elements, so that the absorption process is spread over a large heat transfer area and local overheating is prevented;
- introduce an effective convection heat transfer, with strong 3D flow mixing; the convective cooling pattern should match the distribution of the absorbed radiation;
- be durable and minimize the development of thermal stresses.

The *Porcupine* Absorber

A schematic view of the *Porcupine* absorber is presented in Figure 1. It is an array of *Pin-Fins*, constructed with elongated heat transfer elements (i.e., the *Porcupine* 'quills'), implanted in a base plate. The quills may be made of ceramic tubes or rods and the base is made of a relatively soft ceramic insulation board. The orientation of the pins is designed to match the mean direction of the incoming radiation, and the spacing between them is determined so that the desired radiative flux penetration into the depth of the absorber is obtained (Doron and Kribus, 1997).

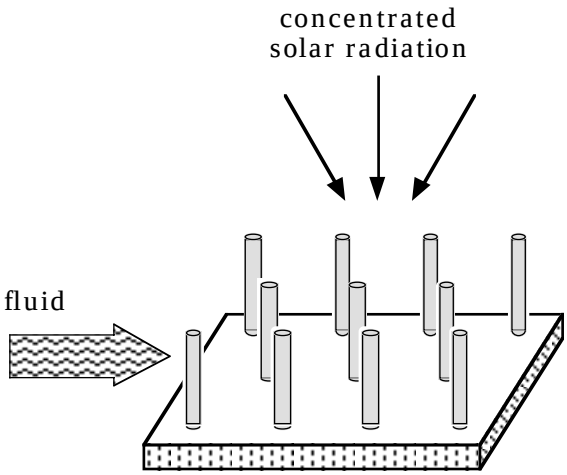

Figure 1. The *Porcupine* Volumetric solar absorber concept.

In all the other stationary absorbers mentioned previously, the flow is in the general direction of the incoming light, as shown schematically in Figure 2(a). In the *Porcupine* the tubular elements are roughly aligned with the irradiation, and the mean flow direction is perpendicular to both (i.e., cross-flow; Figure 2(b)). The latter configuration allows better flexibility in the design of the flow inlet and outlet ports. Thus, the convective cooling, which varies laterally and along the elements, can be matched better with the irradiation flux distribution over the absorber. The cross-flow pattern introduces turbulent mixing and enhances the rate of convective heat transfer from the absorber matrix to the fluid. This is a similar mechanism to that used in many convective heat exchangers, which incorporate tube bundles or *pin fins* in cross-flow.

In the *Porcupine* configuration sunlight can penetrate and be absorbed along the elements. Analysis of the irradiation distribution and its effect on the absorption of the *Porcupine* and other volumetric absorbers was presented by Doron and Kribus (1997). The view-angle between different elements and element parts is large, providing excellent lateral radiation interchange. Since the supporting base plate is relatively soft, the absorber elements are mechanically independent, and each element is free to expand and contract as the temperature varies, hence, no significant thermal stresses can develop.

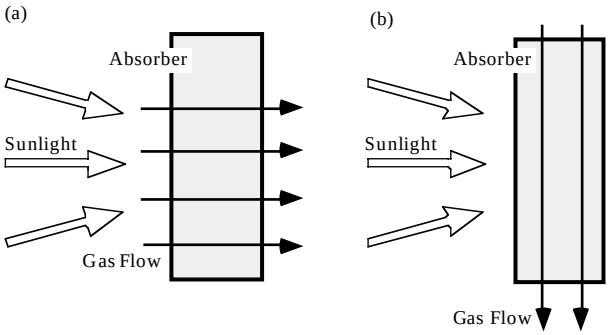

Figure 2. Incident radiation and flow directions in absorbers (a) the incoming sunlight and the working-fluid flow are in the same general direction, as in Foam, Honeycomb, Grid, etc.; (b) the flow is perpendicular to the irradiation, as in the *Porcupine*.

Experimental Setup

Various *Porcupine* absorbers have been tested at the Solar Furnace and Solar Tower of the Weizmann Institute of Science (WIS) over more than 500 heating and cooling cycles. Furnace experiments are reported here; they were designed to gain understanding of the absorber performance. In subsequent experiments the *Porcupine* was incorporated into the *Directly Irradiated Annular Pressurized Receiver* (DIAPR); see Karni et al. (1996) and Karni et al. (1997) for details.

A schematic view of the experimental setup at the Solar Furnace is shown in Figure 3. A flat heliostat tracks the sun and reflects sunlight onto a fixed parabolic-dish concentrator. This radiation is then reflected from the concentrator onto its focus, where over 90% of the light (10–15 kW) is contained in a circular 100 mm diameter plane. The tested absorber is installed inside a quartz bell jar positioned along the symmetry line of the dish. The flux distribution reaching the absorber can be varied by moving the absorber horizontally along the symmetry line to different distances from the focal plane. At the focal plane, it is a nearly rotational symmetric Gaussian distribution, reaching a peak concentration of about 10,000 at the inner 20 mm diameter. As the target is shifted horizontally away from the focus, the peak concentration is reduced, while the illuminated spot is spread over a larger circular plane. Flux profiles at several distances of the target behind the focus were measured using a calorimeter by Rosin et al. (1986). Flux distributions for several positions relative to the focal plane are presented in Figure 4. The total power reaching the focal plane can be varied by changing the door opening of the Furnace. This is represented by the door attenuation factor D=1, 0.935 and 0.706 for door opening of O=6 m (maximum power), 5 and 4 m, respectively (Noter, 1988). Although the door opening also affects the flux distribution, this has little effect on the average absorber performance.

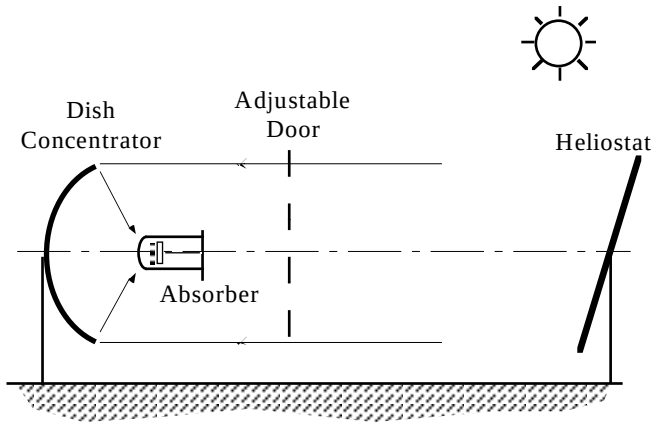

Figure 3. The test setup at the WIS Solar Furnace.

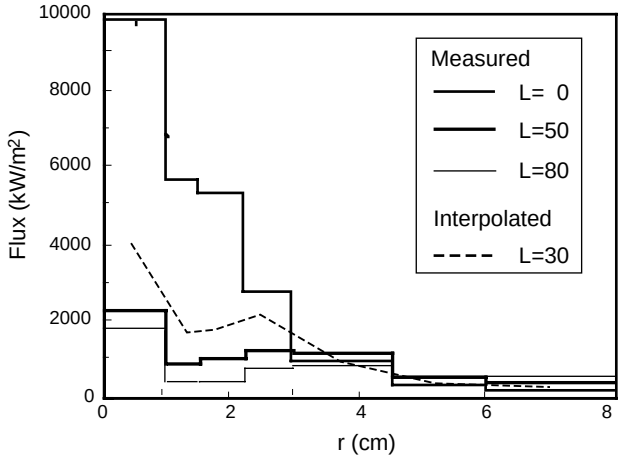

Figure 4. Distribution of local irradiation flux as a function of radius and distance behind the focal plane (after Rosin et. al., 1986); Furnace door opening is O=6 m. Flux values are normalized for incident radiation of 800 W/m^2.

The *Porcupine* absorbers test apparatus is shown schematically in Figure 5. The absorber elements were made of alumina-silica (60% Al_2O_3) tubes, *Pythagoras* (W. Haldenwanger GmbH & Co. KG), or *SL60ZA* (H. Propfe & Co.). In this work we used tubes with ID = 2 mm and OD = 3 mm; in different tests, the quill length was varied from 30 to 60 mm, and the spacing between element centers was 2–8 OD's. These tubes were used mostly because of their commercial availability in the desired dimensions (they are commonly used for high-temperature wire insulation); rods with comparable dimensions would likely produce similar results, although they may have inferior thermal shock resistance. The flat, 144 mm diameter circular base plate was made of *Duraboard HD*™ (Carborundum Resistant Material GmbH), a standard alumina-silica insulation material. The working gas (CO_2) is introduced through an inlet tube located at the center of the base plate, flows radially across the *Porcupine* elements and exits through a symmetric annular gap between the base plate circumference and the bell-jar housing. We estimate the transmissivity of the quartz bell-jar, over the incidence range of 0–65°, as τ=0.92. Four *Porcupine* absorbers with different

inlet configurations and various quill array patterns were studied. Table 1 lists the design characteristics of the absorbers.

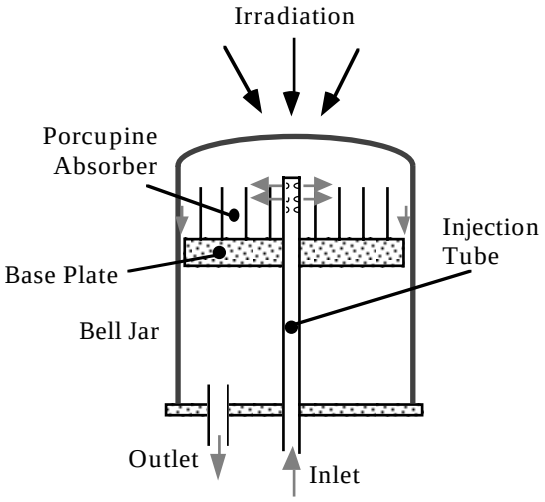

Figure 5. The *Porcupine* absorber experimental apparatus.

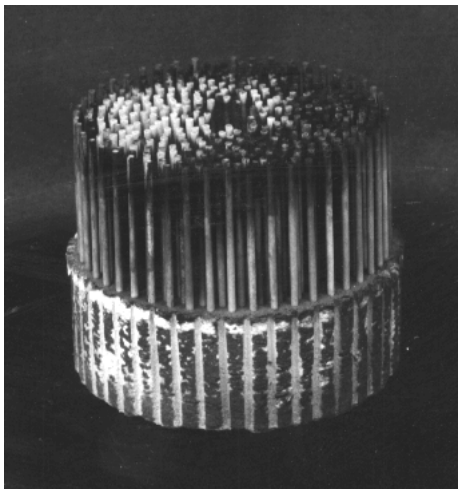

Figure 6. One of the *Porcupine* models (#2) tested at the Solar Furnace.

As seen in Table 1, the main differences between the absorbers are the pin height, injection geometry and pin color. In addition, the pins distribution was varied: in *Porcupines* #2–4 the density of the pins near the center was increased and the density near the periphery was reduced relative to *Porcupine* #1. The changes made between *Porcupine* #2 and 3 were reduction of the number of pins from 432 to 390, to improve the penetration of radiation into the absorber, and variations of the gas inlet geometry. A *Porcupine* model (corresponding to Absorber #2) is shown in Figure 6. Subsequent DIAPR tests (Karni et al., 1996; Karni et al., 1997) used a different *Porcupine* configuration and material, to fit the receiver design and its higher working temperatures.

The inlet flow configurations and thermocouple locations in the elements are shown in Figure 7. Inlet configurations 'S1' and 'S2' of *Porcupine* #1 constituted 13 slots, each 1 mm wide and 30 mm long, evenly spaced around the circumference of an Alumina inlet tube. Inlet configurations 'H1' – 'H4' of *Porcupines* #2 – 4 constituted 12 evenly spaced rows of holes (diameter 1 mm, pitch 2 mm), distributed uniformly around the circumference of an Inconel inlet tube.

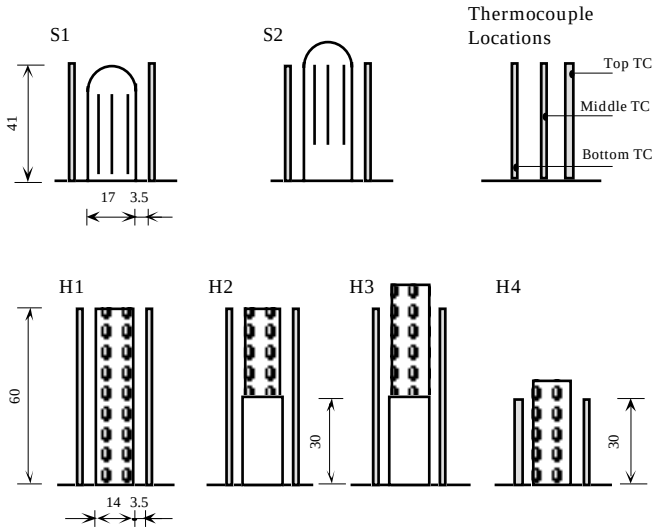

Figure 7. Thermocouple locations in the absorber elements and inlet tube configurations used in tests. S1 - slots with upper edge below quill tops; S2 - slots with upper edge at same elevation as quill tops; H1 - injection holes along the entire 60 mm quill length; H2 - injection holes at the upper 30 mm of the inlet tube only (half of the quill length); H3 - injection holes at the upper 30 mm of the inlet tube, with two additional rings of holes raised above the pin tops; H4 - injection holes along the entire 30 mm quill length and two rings of holes raised above the pin tops.

25 Type K Thermocouples (TC's) were mounted inside the *Porcupine* elements. They were distributed around the absorber, mostly in groups of two or three. In each group of three, the TC's (labeled 'Top,' 'Middle,' and 'Bottom') were inserted at different positions inside adjacent quills, as shown in Figure 7. 'Top' TC's were positioned 1–2 mm below the quills top, 'Middle' TC's were located halfway along the quills, and 'Bottom' TC's were installed 1–2 mm above the Base Plate level. Groups of two included only 'Top' and 'Bottom' TC's. To assure that direct light did not affect 'Top' thermocouple readings, tests were repeated while some of them were covered with alumina cement; no significant deviations in the measurements were detected. One TC was installed in the inlet tube, and 3 TC's were located in the flow outlet gap, between the absorber base plate and the bell jar (Figure 5).

The estimated measurement accuracy is about 3% for of the gas mass flow rate ($\dot{m}$) and average outlet temperature (T_{out}), and about 5% for the power output (Q_{out}) and incident flux (I_n: the flux of normal, non-concentrated radiation).

The incident irradiation power and flux are determined by measuring the direct normal insolation (I_n), interpolating the Solar Furnace concentration data of Rosin et al. (1986) for a given radius r and position L behind the focus to yield the flux concentration $C(r,L)$, and applying the correction factors for

door opening, D, and transmissivity of the bell-jar, τ. The power incident on a circle of radius r is then:

$$Q_{in}(r) = \pi r^2 C(r,L)\tau D(O) I_n \quad (1)$$

Power output (Q_{out}) is calculated from the measured gas inlet and exit temperatures and the mass flow rate. The overall absorber efficiency η is defined relative to the power incident on the entire absorber, within radius R:

$$\eta = \frac{Q_{out}}{Q_{in}(R)} \quad (2)$$

Estimates of local η values, i.e., ratio of absorbed flux to incident flux on small regions of the absorber, show that the variation of η is small. We assume therefore a constant value for further analysis, and the average absorbed flux, $I_{abs}(r)$, within a circle of radius r is estimated as:

$$I_{abs}(r) = \frac{\eta Q_{in}(r)}{\pi r^2} = \eta C(r,L)\tau D(O) I_n \quad (3)$$

Test Results

Tests carried out with the different *Porcupine* configurations are reported. An additional test series was performed with Foam and Honeycomb absorbers, and these results are compared to the performance of the *Porcupine* under similar conditions. Representative test results with the *Porcupine* absorbers are summarized in Table 2. Results with the Foam and Honeycomb absorbers are given in Table 4. Temperature distributions within the absorber elements as well as inlet and outlet temperatures for several test runs are presented below; in these figures, r/R is the relative distance from the absorber's center, i.e., local radial position divided by the absorber's radius. The thermocouple locations within the *Porcupine* elements are as shown in Figure 7.

1.1. Tests with *Porcupines* #1, 2 and 3

In the first test series with *Porcupine* #1, the absorber layout and cooling flow configuration could not adequately match the irradiation flux. Consequently the absorber efficiency and its power yield were relatively low (η=0.34±0.02). Based on the tests, several structural modifications were gradually incorporated into subsequent *Porcupines* to improve performance (see Table 1); the changes included:

1. Improved cooling gas inlet configuration (Figure 7).
2. Better layout of the *Porcupine* pins to provide more effective heat transfer surface area, especially in the inner part of the absorber, where the concentration of incoming radiation is the highest (Figure 4).
3. Coating of the heat transfer surfaces to improve absorptivity; this had a relatively small effect on the performance.

Representative test results with *Porcupine* #2 and #3 are summarized in Table 2. The efficiency of *Porcupine* #2 was higher than that of the first model: η=0.42±0.04. The latter *Porcupine* #3 provided an even higher efficiency: η=0.53±0.06; it also allowed operation at a higher local irradiation flux, i.e., nearer to the focal plane (0 ≤ L ≤ 30 mm) and with the Furnace door fully open (O = 6 m). Overall, *Porcupine* #3 yielded up to 78% more power than #1. The best power output yields obtained with *Porcupine* #3 were 6 kW at outlet gas temperature of 860°C, and 7 kW at outlet gas temperature of 700°C.

Figure 8 and Figure 9 show the effect of changing inlet configuration and pin density. Absorber performance was improved in *Porcupine* #3 by providing a better match between the irradiation flux distribution and the convective heat transfer to the working fluid.

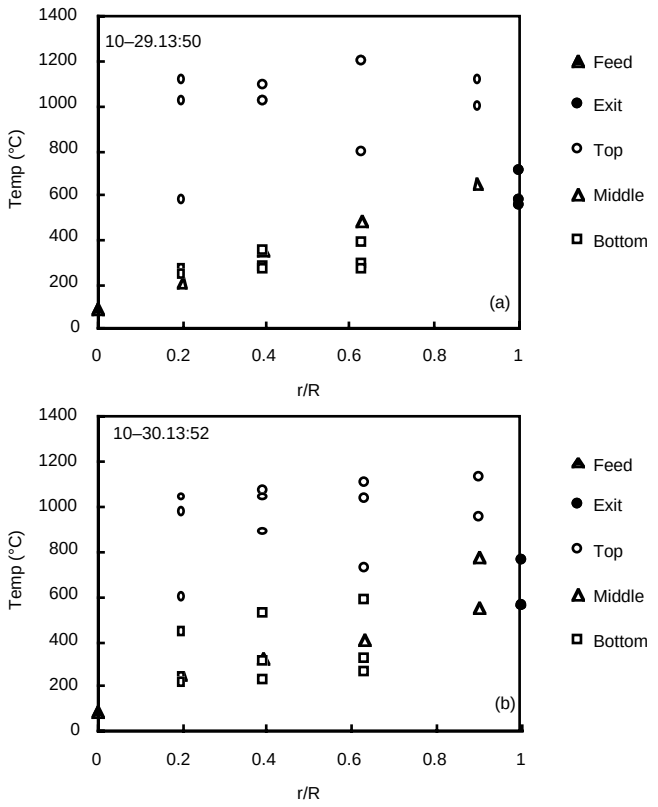

Figure 8. Temperature distributions for *Porcupine* #2. L=30 mm; (a) Inlet configuration H1; I_n=660 W/m^2, $\dot{m}$=6.16·10^{-3} kg/s, O=4 m. (b) Inlet configuration H2; I_n=675 W/m^2, $\dot{m}$=6.18·10^{-3} kg/s, O= 4 m.

Figure 8 shows temperature distributions for *Porcupine* #2. The average exit gas temperature of only 597°C in Figure 8(a) indicates poor heat transfer from the pins to the gas. Also observed is a temperature drop of up to 800°C over a distance of 30 mm from the pin top to its middle. In the lower half of the pins the temperature variation is much smaller. The distribution implies that a relatively small amount of irradiation penetrates deep among the absorber elements. This is typical of off-design conditions, which could occur when the solar heating is non-uniform and the convective cooling does not match the insolation distribution. Such temperature gradients of several hundreds °C/cm, which would have damaged other ceramic matrices, had no adverse effect on the *Porcupine*. In Figure 8(b), the inlet configuration was changed from H1 to H2, where the bottom half of the inlet tube is blocked, forcing all of the gas to

enter through the top part. The top pin temperatures at r/R = 0.2 are about 100°C lower in Figure 8(b) relative to 8(a), indicating some improvement of the heat transfer rate in the high flux region near the absorber center. There is, however, only a negligible effect on the temperature field in the lower half of the pins and little effect on the exit gas temperature: 625°C instead of 597°C.

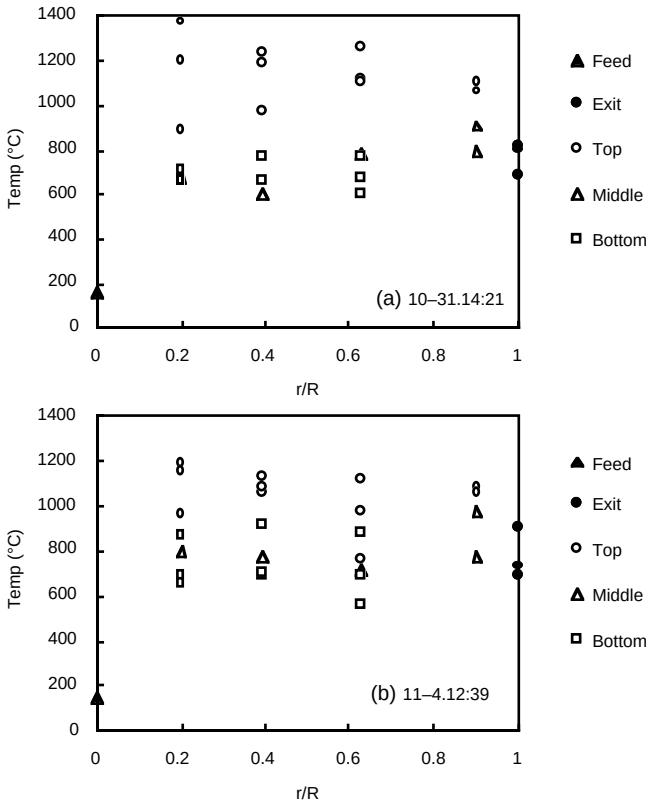

Figure 9. Temperature distributions for *Porcupine* #3. L=30 mm; (a) Inlet configuration H2; I_n=674 W/m^2, $\dot{m}$=6.18·10^{-3} kg/s, O=6 m. (b) Inlet configuration H3; I_n=730 W/m^2, $\dot{m}$=7.38·10^{-3} kg/s, O=6 m.

In *Porcupine* #3 the number of elements was reduced from 432 to 390: half of the pins were removed in the first, third and eighth rings, where the spacing between pins had been relatively small. In the test presented in Figure 9(a) the inlet configuration is H2, like that of Figure 8(b), but with door opening of O=6 m, instead of 4 m, allowing the power that reaches the absorber to increase by about 40%. The smaller number of pins in *Porcupine* #3 enables better penetration of radiation into the absorber, resulting in a significant increase of the temperature in the lower portion of the pins and smaller temperature variations along the pins, despite the higher radiation flux. The average exit gas temperature and the power output obtained in the test of Figure 9(a) are higher by 23% and 28%, respectively, than the corresponding values of Figure 8.

Further improvement was achieved by using inlet configuration H3 with *Porcupine* #3, as shown in Figure 9(b). The power output in this test is 20% higher than that of Figure 9(a), although the incident solar flux increases by only 8%; the average exit gas temperature rises slightly, from 766°C to 778°C, despite the increase in flow rate. The raised injection holes provide better cooling of the pin tips, and the temperature peaks and the temperature differences along the pins are lower in this run than in any of the previous tests.

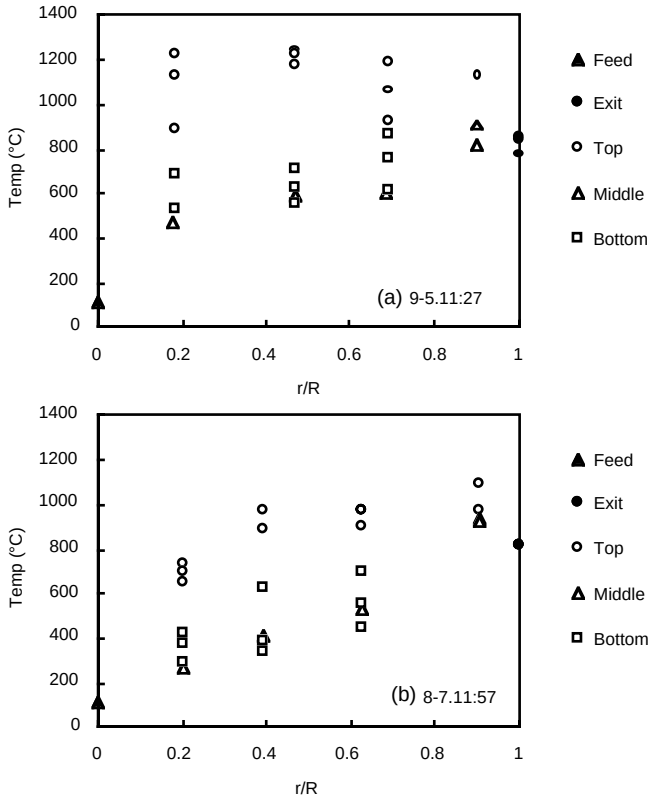

Figure 10. Temperature distributions in *Porcupine* #4 with inlet H4, O=6 m. (a) L=30 mm, I_n=784 W/m^2, $\dot{m}$=11.7·10^{-3} kg/s. (b) L=100 mm, I_n=815 W/m^2, $\dot{m}$=7.36·10^{-3} kg/s.

1.2. Tests with *Porcupine* #4

The absorber elements layout of *Porcupine* #4 is similar to that of #3, but the length of the pins is 30 mm instead of 60 mm and the pins' color is white, not dark brown (Table 1). As observed in earlier tests with *Porcupine* #1, 2 and 3, the front portion of the pins (i.e., near their 'Top') receives most of the incoming radiation. Shortening the pins forces more gas to flow in the front region, improving the convective heat transfer in the region where most of the incoming radiation is absorbed. The inlet configuration used with *Porcupine* #4 was always H4, i.e., the upper two rings of injection holes were protruding above the pin tops (Figure 7). Experimental results obtained with *Porcupine* #4 are presented in Table 2 and Figure 10. The average efficiency achieved with this absorber, η=0.79±0.08, was much higher than that of the previous series. Consequently, the flow rate in *Porcupine* #4 tests could be made considerably higher than in the previous ones, yet the gas exit temperature was higher for similar solar input. This improved performance is obtained although the peak *Porcupine* #4 temperatures are similar to those

of *Porcupine* #3; see for example Figure 10(a) and Figure 9(b), respectively. Note that the change in quills color between *Porcupines* #2, 3 & 4 had little if any effect on performance; the overall *Porcupine* absorption apparently depends mostly on its geometry, not its color.

1.3. Comparison Tests with Foam and Honeycomb Absorbers

Experiments were conducted using the Honeycomb and Foam absorbers shown in Figure 11. In both cases the experimental setup was similar to that shown in Figure 3 and Figure 5. The working gas entered through a central, open-end tube, which penetrated the entire Foam thickness and half of the Honeycomb thickness. Thus, the cold, incoming gas flowed first into the region between the absorber and the frontal dome of the bell jar and then back through the absorber, in the general direction of the incident radiation (Figure 2(a)). The main characteristics of the Honeycomb and Foam absorbers are given in Table 3. Test results of these absorbers are summarized in Table 4, and typical temperature distributions are presented in Figure 12. The exit gas temperature of the Foam and Honeycomb was measured in several locations, adjacent to their back side. The 'Top' measurements were taken by thermocouples located about 1–2 mm from the front (facing the incoming sunlight) absorber surface. The 'Bottom' measurements were taken near the opposite (back) surface of the absorber. To assure that direct light did not affect 'Top' thermocouple readings, tests were repeated while some of them were covered with alumina; no significant deviations in the measurements were detected. The melting of the Honeycomb indicates that higher temperatures than those measured by the TC's may have occurred locally in some tests.

During all the tests, the Honeycomb and Foam absorbers were kept at a distance of 57 or 100 mm from the furnace focus, to avoid exceeding the thermocouples' maximum working temperature of 1350°C. Consequently, they were exposed to lower solar fluxes (maximum of roughly 1000–1500 suns), producing lower output temperatures and power yields than the *Porcupine*. The absorber efficiencies in the Honeycomb and Foam tests were $\eta=0.50\pm0.18$ and 0.59 ± 0.04, respectively. In spite of the relatively low incident flux, the Honeycomb was damaged by local melting (Figure 11) and the Foam developed small cracks near its center. The *Porcupine* absorbers, operating under similar and considerably higher solar flux, showed no signs of deterioration.

The Foam and Honeycomb tests shown in Figure 12 can be compared to the test of *Porcupine* #4 shown in Figure 10(b), which was performed under similar conditions of incident flux and gas flow rate. The efficiency of the *Porcupine* was 0.87, compared to 0.68 and 0.56 for the Foam and Honeycomb, respectively. The exit gas temperature of the *Porcupine* was 830°C, compared to 547°C and 561°C for the Foam and Honeycomb, respectively. The maximum ('Top') absorber temperatures of the *Porcupine* are significantly lower than those of the Foam and Honeycomb, especially near the center. This is due to the better match of convective cooling to the irradiation flux distribution, and better penetration of sunlight into the absorber. Consequently, *Porcupine* #4 was able to achieve both higher efficiency and higher exit temperature than those realized with the Foam and Honeycomb absorbers.

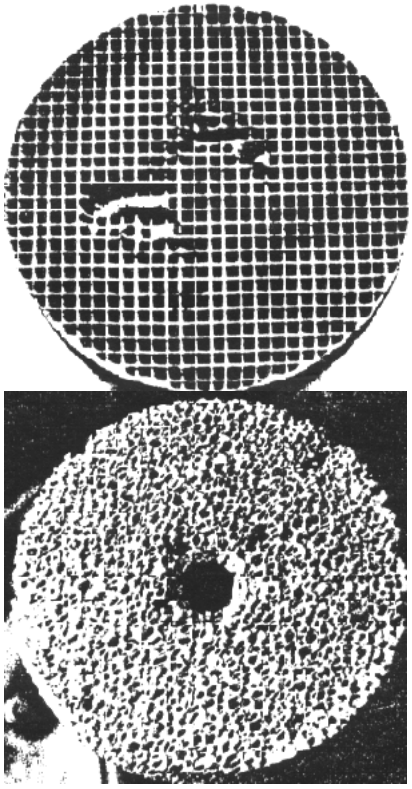

Figure 11: Alternative absorbers: (a) Honeycomb (showing regions where the absorber melted during tests), and (b) Foam.

In the Foam and Honeycomb most of the irradiation is absorbed at the front part of the absorber, but unlike the *Porcupine*, the gas flows into the absorber, not across it (Figure 2). In the present Foam and Honeycomb tests the gas was introduced via the space in front of the absorber, and there was no attempt to adjust the flow field to match the absorbing pattern. Development of similar absorbers is described in many studies; see for example, Buck et. al. (1991), Bauer et. al. (1994), Chavez et. al. (1994), Haeger et. al. (1994), Abele et. al. (1996), and Buck et. al. (1996) Hoffschmidt et al. (1996), Pitz-Paal et. al (1997). In these studies, performance improvement was achieved by means of matrix geometry optimization, material upgrade, inlet flux management and flow/pressure field control. The maximum incident flux was in the range of 700–1000 kW/m^2 and the exit gas temperature was in the range 500–900°C. These are comparable to the results of the (un-optimized) Foam and Honeycomb absorbers reported here.

Figure 13 shows a comparison of exit gas temperature and power transferred to the working gas as a function of the cooling gas mass flow rate, for the Honeycomb, Foam and *Porcupine* #3 and #4. The Figure includes only test results where the maximum flux levels were approached, i.e., the peak thermocouple readings

approached the maximum working temperature (1,350°C), and yielded relatively high power output and exit gas temperature. These selected results represent therefore the *performance envelope* of the different absorbers under the given test constraints. The power yield of *Porcupine* #4 was about 100% higher than those of the Honeycomb and Foam (which were quite close to each other) and 30–40% higher than that of *Porcupine* #3. The exit gas temperature of *Porcupine* #4 was 300–350°C and 150–200°C higher of those of the Foam & Honeycomb, and *Porcupine* #3, respectively.

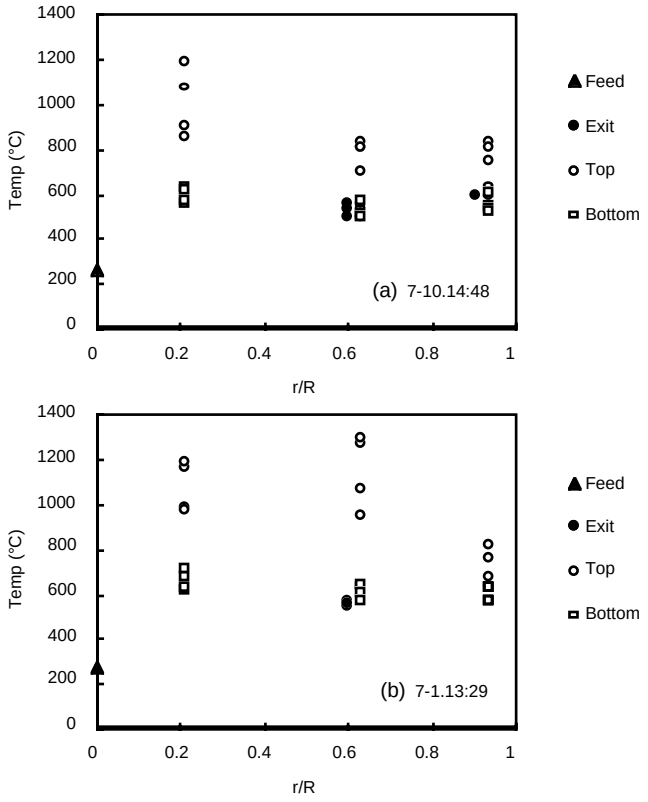

Figure 12. Temperature distribution in Foam and Honeycomb absorbers. O=6 m; L=100 mm. (a) Foam, I_n=775 W/m^2, $\dot{m}$=7.36·10^{-3} kg/s. (b) Honeycomb, I_n=821 W/m^2, $\dot{m}$=7.33·10^{-3} kg/s.

Conclusions

A new Directly-Irradiated (Volumetric) absorber, the *Porcupine*, was constructed and tested at the Solar Furnace of the Weizmann Institute. The main advantages of the *Porcupine* absorber are:

- Good energy transport capability along each pin and among neighboring pins, which prevents local overheating.
- High rate of convective heat transfer between the absorber and the working fluid.
- Flexibility in distribution and control of the flow and absorber temperature.
- Extremely high durability and inherent resistance to the development of thermal stresses.
- Easy adaptation to solar driven thermo-chemical processes such as hydrocarbons reforming, by coating the *Porcupine* pins with a catalyst.

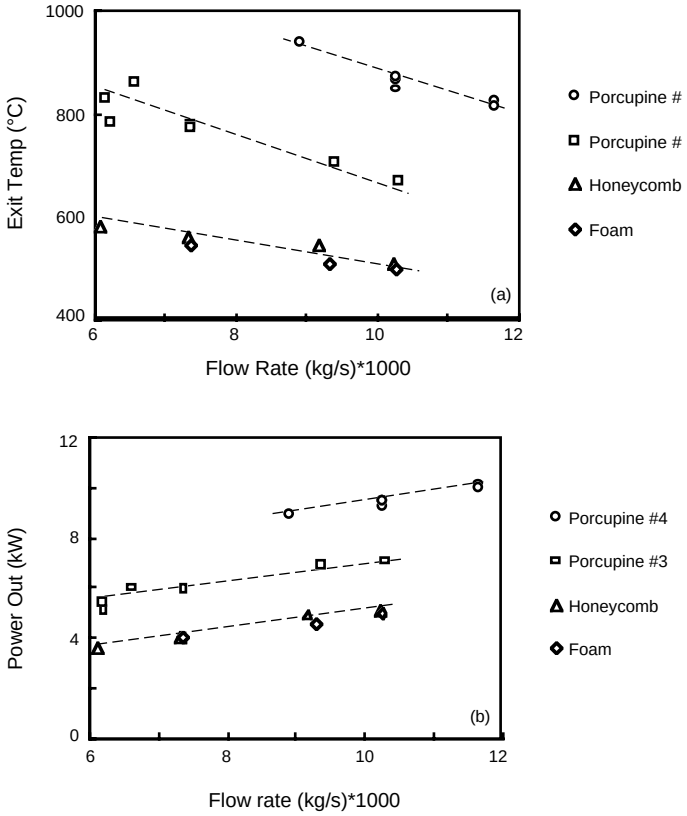

Figure 13. Comparison of (a) exit gas temperature and (b) power output of the Honeycomb, Foam and two *Porcupine* absorbers. Only tests where absorber temperature approached the maximum allowed limit are included.

In tests at the WIS solar furnace, the latest version of the *Porcupine* (#4) withstood up to 4 MW/m^2 of incident radiation at maximum absorber temperature of 1,300–1,400°C, while transferring up to 3 MW/m^2 of it to the working gas. Power output of 9 kW at exit gas temperature of 940°C, and 10 kW at exit gas temperature of 820°C was obtained. Absorber efficiency of about 0.80 was achieved within this temperature range. Commonly used alternative absorbers, Honeycomb and Foam matrices, were also tested under similar conditions to those in the *Porcupine* experiments. The peak power yields obtained with these absorbers were about 50% of those measured with *Porcupine* #4, while their exit gas temperature was 300–350°C lower. These absorbers withstood a maximum solar flux of about 1–1.2 MW/m^2, while transporting up to 0.5–0.7 MW/m^2 of it to the cooling gas; these are about 20–30% of the maximum solar flux absorbed and transferred, respectively, to the coolant by *Porcupine* #4. Absorber efficiencies in the range of 0.50–0.60 were obtained with these absorbers, much lower than that of the *Porcupine*. The comparison shows that the Porcupine provides better performance under similar conditions, and a much wider operation envelope in terms of exit temperature and

incident flux. There was no attempt to optimize the performance of the Honeycomb and Foam absorbers, but their present measured performance was comparable to other reported data with similar absorbers, where optimization was attempted.

The performance of the *Porcupine* absorber is sensitive to the details of the fluid inlet and the pins layout. The *Porcupine* design therefore provides a means for matching between the irradiation intensity distribution and the distribution of convective cooling, consequently, local overheating is reduced. Significant improvement in performance was demonstrated by manipulation of the absorber and fluid inlet geometry.

The *Porcupine* structure of mechanically independent members annuls thermal stresses development; consequently, cracking of the absorber material is prevented. Temperature gradients of about 800°C/cm, which developed in early tests, did not damage the *Porcupine* matrix. None of the *Porcupine* absorbers showed any signs of deterioration after hundreds of operating hours.

Test results at higher operating temperatures, showing further improvement in the *Porcupine* performance, especially its ability to allow penetration of incident radiation into it and provide good radiative exchange between the absorbing elements, were described by Karni et. al. (1996).

The *Porcupine* absorber is patented by Yeda Research & Development, Ltd.

Acknowledgment

This work was funded by the Israel Ministry of Energy and Infrastructure.

References

Abele, M., Bauer, H., Buck, R., Tamme, R. and Wörner, A., 1996, "Design and Test Results of a Receiver–Reactor for Solar Methane Reforming," *Proceedings of ASME Solar Engineering 1996, The 1996 International Solar Energy Conference,* pp. 339–346.

Andraka, C.E., Adkins, D.R., Moss, T.A., Cole, H.M. and Andreas, N.H., 1995, "Felt-Metal-Wick Heat-Pipe Solar Receiver," *Proceedings of Solar Engineering 95, the 1995 ASME/JSME/JSES International Solar Energy Conference*, Maui, Hawaii, Vol. 1, pp. 559–564.

Anikeev, V.I., Bobrin, A.S. and Kirillov, V.A., 1992, "New Conception of Catalytic Volumetric Reactor-Receiver," *Proceedings of the 6th International Symposium on Solar Thermal Concentrating Technologies,* Vol. 1, pp. 387–394.

Bauer, H. Abele, M., Biehler, T., Buck, R. and Heller, P., 1994, "Design and Test of Volumetric Receivers for Dish/Brayton Systems and Solar Methane Reforming," *Proceedings of the 7th International Symposium on Solar Thermal Concentrating Technologies*, Vol. 4, pp. 818–825.

Böhmer, M. and Chaza, C., 1991, "The Ceramic Foil Volumetric Receiver," *Solar energy Materials*, Vol. 24, pp. 182–191.

Buck, R., 1990, "Test and Calculations for a Volumetric Ceramic Receiver," *Solar Thermal Technology–Research Development and Applications, Proceedings of the 4th International Symposium,* B.P. Gupta, W.H. Traugott eds., Hemisphere Publishing Corp., New York, pp. 279–286.

Buck, R., Muir, J.F., Hogan, R.E. and Skocypec, R.D., 1991, "Carbon Dioxide Reforming of Methane in a Solar Volumetric Receiver/Reactor: the CAESAR Project," *Solar Energy Materials,* Vol. 24, pp. 449–463.

Buck, R., Heller, P. and Koch, H., 1996, "Receiver Development for a Dish-Brayton System," *Proceedings of ASME Solar Engineering 1996, The 1996 International Solar Energy Conference,* pp. 91–96.

Chavez, J.M., Tyner, C.E. and Couch, W.A., 1990, "Direct Absorption Receiver Flow Testing and Evaluation," *Solar Thermal Technology–Research Development and Applications, Proceedings of the 4th International Symposium,* B.P. Gupta, W.H. Traugott eds., Hemisphere Publishing Corp., New York, pp. 645–654.

Chavez, J.M., Lessley, R.L. and Leon, J., 1994, "Design, Fabrication and Testing of a 250kWt Knit-Wire Mesh Volumetric Air Receiver," *Proceedings of the 1994 ASME/JSME/JSES International Solar Energy Conference,* pp. 605–610.

Diver, R.B., Fish, J.D., Levitan, R., Levy, M., Meirovitch, E., Rosin, H., Paripatyadar, S.A. and Richardson, J.T., 1992, "Solar Test of an Integrated Sodium Reflux Heat Pipe Receiver/Reactor for Thermochemical Energy Transport," *Solar Energy,* Vol. 48, No. 1, pp. 21–30.

Doerte, L. and Goebel O., 1992, "Sodium Heat Pipe Receiver for a SPS V 160 Stirling Engine: Second Generation Design," *Proceedings of the 6th International Symposium on Solar Thermal Concentrating Technologies,* Vol. 1, pp. 427–434.

Doron, P. and Kribus, A., 1997, "The Effect of Irradiation Directional Distribution on Absorption in Volumetric Solar Receivers," *ASME J. of Solar Energy Engineering,* Vol. 119, Feb. 1997 (in press).

Epstein, M., 1990, "Solar Tests of a Ceramic Tubes Receiver at the Weizmann Institute of Science Solar research Facilities–Status Report," *Solar Thermal Technology–Research Development and Applications, Proceedings of the 4th International Symposium,* B.P. Gupta, W.H. Traugott eds., Hemisphere, pp. 231–234.

Flamant, G. and Olalde, G., 1983, "High Temperature Solar Gas Heating Comparison Between Packed and Fluidized Bed Receivers–I," *Solar Energy*, Vol. 31, pp 463–471.

Fletcher, E. A., and Moen, R. L., 1977, "Hydrogen and Oxygen from Water," *Science*, Vol. 197, pp. 1050–1056.

Fricker, H.W., Winkler, C., Silva, M. and Chavez, J., 1990, "Design and Test Results of the Wire Receiver Experiment Almeria," *Solar Thermal Technology–Research Development and Applications, Proceedings of the 4th International Symposium,* B.P. Gupta, W.H. Traugott eds., Hemisphere, pp. 265–277.

Haeger, M., Meinecke, W. and Cordes, S., 1994, "Phoebus Technology Program Solar Air Receiver (TSA)–Operational Experience and Test Evaluation of the 2.5MW_{th} Volumetric Air Receiver Test Facility at the Plataforma Solar de Almeria," *Proceedings of the 7th International Symposium on Solar Thermal Concentrating Technologies,* Vol. 4, pp. 943–957.

Heinrich, P., Keintzel, G. and Streuber, C., 1992, "Technology Program Solar Air Receiver–2.5MW_t System Test on Volumetric Air Receiver Technology," *Proceedings of the 6th International Symposium on Solar Thermal Concentrating Technologies,* Vol. 1, pp. 247–261

Hellmuth, T.E., Matthews, L.K., Chavez, J.M. and Hale, C.A., 1994, "Performance of a Wire Mesh Solar Volumetric Air Receiver," *Proceedings of the 1994 ASME/JSME/JSES International Solar Energy Conference,* pp. 573–578.

Hoffschmidt, B., Pitz-Paal, R. and Böhmer, M., 1996, "Porous Structures for Volumetric Receivers–Comparison of Experimental and Numerical Results," *8th International Symposium on Solar Thermal Concentrating Technologies*, Köln, Germany, October 1996.

Hunt, A.J., and Brown, C.T., 1984, "Solar Test Results of an Advanced direct Absorption High Temperature Gas Receiver (SPHER)," *Solar World Congress 1983, Proceedings of the 8th Biennial Congress of the ISES*, Szokolay, S.V., ed., Pergamon Press, Oxford, UK, Vol. 2, pp. 959–963.

Karni, J., Rubin, R., Kribus, A., Doron, P. and Sagie, D., 1996, "Test Results with the Directly-Irradiated Annular Pressurized Receiver," *8th International Symposium on Solar Thermal Concentrating Technologies*, Köln, Germany, October 1996.

Karni, J., Kribus, A., Rubin, R., Doron, P., Fiterman, A. and Sagie, D., 1997, "The DIAPR: A High-Pressure, High-Temperature Solar Receiver," *ASME J. of Solar Energy Engineering,* Vol. 119, pp. 74–78.

Klimas, P.C., Andraka, C.E. and Moreno, J.B., 1992, "The U.S.-DOE Reflux Receiver Development Program," *Proceedings of the 6th International Symposium on Solar Thermal Concentrating Technologies,* Vol. 1, pp. 409–425.

Kribus, A., Ries, H. and Spirkl, W., 1996, "Inherent Limitations of Volumetric Solar Receivers," *ASME J. of Solar Energy Engineering,* Vol. 118, 151–155.

León, J., Sánchez-Jiménez, M., Sánchez-Gonzalez, M., Romero, M. and Barrera, G., 1994, "Design and First Tests of an Advanced Salt Receiver Based on the Internal Film Concept," *Proceedings of the 7th International Symposium on Solar Thermal Concentrating Technologies,* Vol. 4, pp. 921–933.

Levy, M., Rosin, H. and Levitan, R., 1989, "Chemical Reactions in a Solar Furnace by Direct Solar Irradiation of the Catalyst," *ASME J. of Solar Energy Engineering*, Vol. 111, 96.

Litwin, R.Z., and Rogers, R.D., 1996, "Fabrication and Installation of the Solar Two Central Receiver," *Proceedings of ASME Solar Engineering 1996, The 1996 International Solar Energy Conference*, pp. 125–132.

Menigault, T., Flamant, G. and Rivoire, B., 1991, "Advanced High-Temperature Two-Slab Selective Volumetric Receiver," *Solar Energy Materials*, Vol. 24, pp. 192–203.

Noble, J.E., Olan, R.W., White, M.A., Kesseli, J., Bohn, M.S., Scholl, K.L. and Becker, E.W., 1995, "Test Results from a 10 kW_t Solar/Natural Gas Hybrid Pool Boiler Receiver," *Proceedings of Solar Engineering 95, the 1995 ASME/JSME/JSES International Solar Energy Conference*, Maui, Hawaii, Vol. 1, pp. 565–573.

Noter, Y., 1988, "Characterization of the Solar Spot at the Solar Furnace." Weizmann Institute of Science internal report.

Olalde, G., Flamant, G., Schwander, D. and Combescure, C., 1985, "Advance high-Temperature Semi-Transparent Solar Absorbers," *Solar energy Materials*, Vol. 12, pp. 461–469

Pitz-Paal, R., Morhenne, J. and Fiebig, M., 1991, "Optimization of the Surface Geometry of a Volumetric Foil Receiver," *1991 Solar Energy World Congress*, Vol. 2 Part II, pp. 1999–2004.

Pitz-Paal, R., Fiebig, M. and Cordes, S., 1992, "First Experimental Results from the Test of a Selective Volumetric Air Receiver," *Proceedings of the 6th International Symposium on Solar Thermal Concentrating Technologies*, Vol. 1, pp. 277–289.

Pitz-Paal, R., 1996, "Evaluation of the CATREC II Receiver Test," *IEA Solar PACES Technical Report*, No. III-2/96.

Pitz-Paal, R., Hoffschmidt, B., Böhmer, M. and Becker, M., 1997, "Experimental and Numerical Evaluation of the Performance and Flow Stability of Different Types of Open Volumetric Absorbers Under Non-Homogeneous Irradiation," *Solar Energy*, Vol. 60, pp. 135–150.

Posnansky, M. and Pylkkänen, T., 1992, "High Temperature Volumetric Gas Receiver–Results of the Development and Testing of the Atlantis Ceramic Receiver," *Proceedings of the 6th International Symposium on Solar Thermal Concentrating Technologies*, Vol. 1, pp. 291–298.

Pritzkow, W. E. C., 1991, "Pressure Loaded Volumetric Ceramic Receiver, *Solar Energy Materials*, Vol. 24, pp. 498–507.

Rosin, H., Levy, I. and Levithan, R., 1986, "The Solar Furnace Performance as Measured by Calorimetry." Weizmann Institute of Science internal report.

Smith, D.C. and Allman, W.A., 1990, "The Design of Compact Receivers for Molten Salt SCR Plants," *Solar Thermal Technology–Research Development and Applications, Proceedings of the 4th International Symposium*, B.P. Gupta, W.H. Traugott ed., Hemisphere Publishing Corp., New York, pp. 253–262.

Table 1. Characteristics of the experimental *Porcupine* absorbersw

		Porcupine #1	*Porcupine* #2	*Porcupine* #3	*Porcupine* #4
General	Absorber diameter (mm)	144			
	Distance from front glass to pin-tops (mm)	20			
	No. of TC's (in quills/inlet/exit)	25/1/3			
Quill Elements	No. of quills	390	432	390	390
	Material (types of Alumina-Silica)	Pythagoras	SL60ZA	SL60ZA	Pythagoras
	Color	white	dark brown(1,2)	dark& white(2)	white
	Height (mm)	41	60	60	30
	Diameter – O.D./I.D. (mm)	3/2			
	Maximum working temp. (°C)	1600			
Base Plate	Material	Duraboard HD			
	Color	white	dark brown(1)	dark brown(1)	white
	Thickness (mm)	25	50	50	25
	Maximum working temp. (°C)	1260			
Inlet Tube	Material	Pythagoras	Inconel	Inconel	Inconel
	Diameter – O.D./I.D. (mm)	17/13	14/12	14/12	14/12
	Gas inlet geometry(3)	S1, S2	H1, H2	H2, H3	H4

Notes for Table 1:

(1) The dark brown color was obtained by coating the pins and the base plate with ferric oxide (Fe_2O_3).

(2) The color of the pins in *Porcupine* #2 varied gradually during the tests. The initially dark brown coating gradually evaporated in the hotter regions, and the pins color changed back to white (see Figure 6). These changes had no apparent effect on the absorber's performance, within the resolution of the temperature measurements.

(3) See Figure 7.

Table 2. Summary of test results with *Porcupine* absorbers.

Run No.	O	L	Inlet	I_n	Est. Q_{in}	$\dot{m}$	T_{out}	Q_{out}	Est. Peak Flux (kW/m^2)	
	(m)	(mm)		(W/m^2)	(W)	(kg/s)	(°C)	(W)	Incident	Absorbed
Porcupine #1										
5-15.11:12	6	57	S1	624	7300	$3.75 \cdot 10^{-3}$	673	2600	1560	560
5-16.11:25	6	57	S2	817	9600	$3.75 \cdot 10^{-3}$	809	3180	2070	690
5-16.12:49	6	57	S2	832	9700	$3.73 \cdot 10^{-3}$	805	3150	2120	690
5-16.13:06	6	57	S2	818	9600	$4.47 \cdot 10^{-3}$	761	3540	2070	770
5-16.14:46	4	30	S2	758	8600	$4.47 \cdot 10^{-3}$	589	2640	2480	770
5-16.14:58	6	30	S2	755	12100	$5.10 \cdot 10^{-3}$	723	3840	3500	1110
5-16.15:12	6	30	S2	739	11900	$5.31 \cdot 10^{-3}$	720	3980	3400	1140
Porcupine #2										
10-29.13:28	4	30	H1	690	7800	$6.16 \cdot 10^{-3}$	542	2870	2240	820
10-29.13:50	4	30	H1	660	7500	$6.16 \cdot 10^{-3}$	597	3170	3040	1290
10-29.14:13	4	30	H1	629	7100	$6.13 \cdot 10^{-3}$	574	3040	2890	1240
10-30.13:52	4	30	H2	675	7600	$6.18 \cdot 10^{-3}$	575	3050	3110	1240
10-30.14:07	4	30	H2	651	7400	$6.16 \cdot 10^{-3}$	624	3310	2990	1350
10-30.14:33	4	10	H2	612	7000	$6.19 \cdot 10^{-3}$	629	3340	3580	1710
10-30.14:52	5	10	H2	545	8300	$6.18 \cdot 10^{-3}$	639	3390	4220	1730
Porcupine #3										
10-31.13:23	4	57	H2	800	6600	$4.47 \cdot 10^{-3}$	766	3560	1430	770
10-31.13:50	6	57	H2	750	8700	$6.18 \cdot 10^{-3}$	689	4410	1890	960
10-31.14:10*	6	30	H2	708	11300	$6.21 \cdot 10^{-3}$	781	5080	3260	1460
10-31.14:21	6	30	H2	674	10800	$6.18 \cdot 10^{-3}$	766	4990	3100	1440
10-31.14:59	6	10	H2	570	9400	$6.21 \cdot 10^{-3}$	759	4930	4720	2480
10-31.15:24	6	0	H2	460	7500	$6.18 \cdot 10^{-3}$	684	4365	5180	3000
11-2.10:02*	6	57	H3	885	10300	$6.18 \cdot 10^{-3}$	829	5405	2240	1170
11-2.10:28*	5	30	H3	890	13300	$6.60 \cdot 10^{-3}$	862	6020	3830	1730
11-4.12:39*	6	30	H3	730	11700	$7.38 \cdot 10^{-3}$	778	6010	3360	1730
11-4.12:49*	6	30	H3	726	11600	$7.38 \cdot 10^{-3}$	772	5960	3340	1720
11-4.13:16*	6	20	H3	710	11500	$9.39 \cdot 10^{-3}$	705	6870	4080	2440
11-4.13:40*	6	10	H3	677	11000	$10.3 \cdot 10^{-3}$	669	7100	5600	3600
Porcupine #4										
8-7.11:33	6	100	H4	798	7200	$6.11 \cdot 10^{-3}$	889	5740	920	740
8-7.11:57	6	100	H4	815	7400	$7.36 \cdot 10^{-3}$	830	6390	1030	890
8-7.12:41	6	57	H4	844	9800	$10.3 \cdot 10^{-3}$	847	9200	2130	1990
8-7.13:07*	6	30	H4	827	13200	$10.3 \cdot 10^{-3}$	881	9610	3800	2760
9-4.12:31	6	57	H4	796	9300	$10.3 \cdot 10^{-3}$	782	8370	2010	1810
9-4.13:14	6	30	H4	799	12800	$10.3 \cdot 10^{-3}$	866	9450	3680	2710
9-4.15:21	6	30	H4	792	12700	$10.3 \cdot 10^{-3}$	811	8740	3640	2510
9-5.11:09*	6	30	H4	775	12400	$10.3 \cdot 10^{-3}$	868	9470	3570	2720
9-5.11:27*	6	30	H4	784	12500	$11.7 \cdot 10^{-3}$	824	10130	3610	2920
9-5.11:42*	6	25	H4	781	12600	$11.7 \cdot 10^{-3}$	816	10010	4040	3210
9-5.11:54	6	25	H4	764	12300	$10.3 \cdot 10^{-3}$	871	9510	3960	3050
9-5.12:12*	6	25	H4	775	12500	$8.9 \cdot 10^{-3}$	938	8950	4010	2870

Note: Cases denoted by (*) are included in Figure 13.

Table 3. Characteristics of the experimental Honeycomb and Foam absorbers.

	Honeycomb	Foam
Absorber diameter (mm)	144	144
Absorber thickness (mm)	40	35
Pore shape	square	round or oval
Pore Size/wall thickness (mm)	8x8/1	2<d<10/0.8
Front-glass to absorber-top distance (mm)	20	20
No. of TC's (in absorber/inlet/exit)	25/1/3	24/1/4
Thermocouple locations in absorber	front & back	front & back
Absorber material)	Alumina-Silica	Alumina-Silica
Color	off-white	White
Absorber maximum working temp. (°C)	1500	1600
Inlet tube material	Pythagoras	Pythagoras
Inlet tube diameter – O.D./I.D. (mm)	17/13	17/13
Inlet tube position	absorber center, half-through	absorber center, full-through

Table 4. Summary of Honeycomb and Foam absorbers test results.

Run No.	O (m)	L (mm)	I_n (W/m^2)	Estimated Q_{in} (W)	$\dot{m}$ (kg/s)	T_{out} (°C)	Q_{out} (W)	Estimated Peak Flux (kW/m^2) Incident	Absorbed
Honeycomb									
5-21.14:39	4	100	926	8320	$7.21 \cdot 10^{-3}$	518	3660	740	330
5-23.14:58*	5	100	832	7480	$6.11 \cdot 10^{-3}$	584	3580	890	430
6-30.14:17	4	57	825	9600	$6.72 \cdot 10^{-3}$	415	2630	1470	400
7-1.12:14	4	57	771	8900	$6.11 \cdot 10^{-3}$	455	2660	1380	410
7-1.12:49*	6	100	767	6900	$10.2 \cdot 10^{-3}$	510	5110	880	660
7-1.13:06*	6	100	810	7300	$9.17 \cdot 10^{-3}$	547	4970	940	630
7-1.13:29*	6	100	821	7360	$7.33 \cdot 10^{-3}$	561	4100	950	530
Foam									
7-10.14:31*	6	100	809	7300	$9.31 \cdot 10^{-3}$	507	4610	930	590
7-10.14:48*	6	100	775	6900	$7.36 \cdot 10^{-3}$	547	3990	890	520
7-11.11:29	5	57	671	7800	$10.3 \cdot 10^{-3}$	428	4160	1590	850
7-11.11:41*	5	57	725	8400	$10.3 \cdot 10^{-3}$	501	5020	1710	1030

Note: Cases denoted by (*) are included in Figure 13.